JACS
JOURNAL OF THE AMERICAN CHEMICAL SOCIETY
Article
pubs.acs.org/JACS

Effect of Orientation of the Peptide-Bridge Dipole Moment on the Properties of Fullerene–Peptide–Radical Systems

Luca Garbuio,[†] Sabrina Antonello,[†] Ivan Guryanov,[†] Yongjun Li,[‡] Marco Ruzzi,[†] Nicholas J. Turro,*[,‡] and Flavio Maran*[,†]

[†]Department of Chemistry, University of Padova, Via Marzolo 1, 35131 Padova, Italy
[‡]Department of Chemistry, Columbia University, New York, New York 10027, United States

Supporting Information

ABSTRACT: We synthesized two series of compounds in which a nitroxide radical and a fullerene C_{60} moiety were kept separated by a 3_{10}-helical peptide bridge containing two intramolecular C═O···H–N hydrogen bonds. The direction of the resulting molecular dipole moment could be reversed by switching the position of fullerene and nitroxide with respect to the peptide nitrogen and carbon termini. The resulting fullerene–peptide–radical systems were compared to the behaviors of otherwise identical peptides but lacking either C_{60} or the free radical moiety. Electrochemical analysis and chemical nitroxide reduction experiments show that the dipole moment of the helix significantly affects the redox properties of both electroactive groups. Besides providing evidence of a folded helical conformation for the peptide bridge, IR and NMR results highlight a strong effect of peptide orientation on the spectral patterns, pointing to a specific interaction of one of the helical orientations with the C_{60} moiety. Time-resolved EPR spectra show not only that for both systems triplet quenching by nitroxide induces spin polarization of the radical spin sublevels, but also that the coupling interaction can be either weak or strong depending on the orientation of the peptide dipole. As opposed to the concept of dyads, the molecules investigated are thus better described as fullerene–peptide–radical systems to stress the active role of the bridge as an important ingredient capable of tuning the system's physicochemical properties.

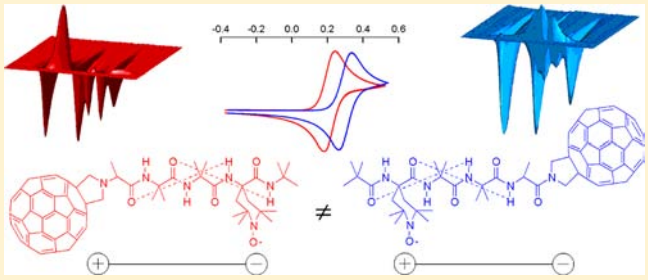

INTRODUCTION

Since its discovery in 1985,[1] the properties of the C_{60} fullerene have been extensively investigated. Thorough understanding of its chemical reactivity has led to the synthesis of a large number of fullerene derivatives whose properties and applications have been studied from many viewpoints.[2] Among them, interesting molecular systems are featured by fullerene–radical dyads where C_{60} is covalently linked, through formation of fulleropyrrolidines,[3] either directly or via a molecular spacer to a free radical function.[4,5] Besides interest in synthesis and properties of C_{60} and its derivatives, endohedral fullerenes[6] in which atom or small molecule is encapsulated in the C_{60} nano cavity have become a field that attracts more attention due to their potential applications in medicine and biology.[7,8] In particular, the recently successful synthesis[9] of $H_2@C_{60}$ by the molecular surgery method makes the material available in quantities from tens to hundreds of milligrams. Therefore, to probe the interactions of the motion of the endohedral molecule with the outside environment,[10] a series of $H_2@C_{60}$ derivatives covalently linked to a nitroxide radical has been synthesized in which the nitroxide moiety acts as a relaxation agent, and the effect of the nitroxide radical on proton nuclear spin relaxation of the endohedral molecule has been investigated.[11]

In this Article, we describe properties and compare the behavior of compounds in which a free radical and a fullerene C_{60} moiety are separated by a peptide. We particularly focused on compounds that show different properties only because of the orientation of the peptide bridge with respect to the above moieties. Our main aim was to explore the effect of reversing the peptide orientation and thus the direction of the dipole moment of the bridge on the spectral, electrochemical, and magnetic properties of the fullerene–radical dyad systems. In this context, some interesting published results are worth mentioning. We previously reported that an oriented peptide dipole moment affects the redox potentials of electroactive groups[12] and even gold nanoparticles.[13] Thanks to the use of stiff helical peptide scaffolds, Galoppini and Fox observed that the rate of photoinduced intramolecular electron transfer is affected by the direction of the peptide dipole moment.[14] Similar results were later obtained on electroactive self-assembled monolayers on gold electrodes.[15] Concerning fullerene derivatives, that the onset of an ordered peptide helical structure affects the way by which donor and acceptor interact was evidenced by Polese et al. in their study about the solvent dependence of intramolecular electron transfer in

Received: April 17, 2012
Published: May 31, 2012

dx.doi.org/10.1021/ja303696s | J. Am. Chem. Soc. 2012, 134, 10628–10637

Chart 1

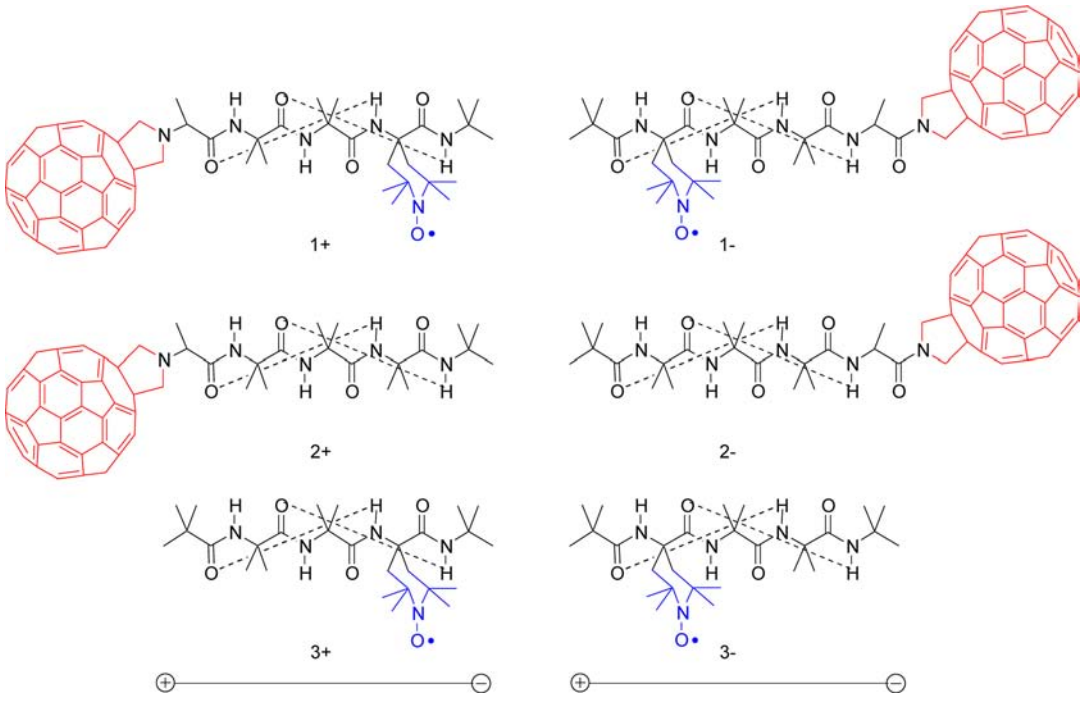

fullerene−peptide−$[Ru(bpy)_3]^{2+}$ systems.[16] In a very recent paper, de Miguel et al. studied the photoinduced electron transfer between zinc(II)porphyrins and fullerenes connected via triazole bridges and reached the conclusion that the nature of the bridge affects charge separation and charge recombination dynamics.[17]

For the purpose of our study, peptides with well-defined features, that is, a definite conformational preference, sufficient stiffness, and a structure causing onset of a strong dipole moment, are required. These properties are collectively possessed by peptides based on the α-aminoisobutyric acid (Aib) residue. Aib is characterized by marked steric hindrance at the α-carbon and restricted torsional freedom.[18] Because of these features, Aib peptides adopt a 3_{10}-helical structure and display the remarkable property that their tendency to form β-turns and 3_{10}-helices is already evident starting from the tripeptide.[18−20] Aib peptides are known to be remarkably rigid even when they are short,[20,21] which is a general feature shared by oligopeptides based on C^{α}-tetrasubstituted α-amino acids.[18] Rigidity is ensured by a framework of intramolecular C═O···H−N hydrogen bonds. These H-bonds force the C═O and N−H groups to align significantly along the peptide axis, and thus formation of the 3_{10}-helix is accompanied by the onset of a strong molecular dipole moment that has its positive pole on the nitrogen terminus of the peptide.[22] The outcome of theoretical calculations is that the dipole moment of 3_{10}-helical peptides changes by 4.5 D/residue[22b] (although individual C═O dipole moments depend on the actual number of residues along the chain),[22c] although experimental determinations of short peptides point to the smaller but still considerable value of ca. 2.3 D/residue.[13] It is worth stressing that although the onset of a strong molecular dipole moment is valid also for other peptide secondary structures, such as the α-helix,[22b] peptides based on coded α-amino acids form stable helices only for rather long oligomers, and thus the dipole moment of short oligomers is much less controlled than in Aib-oligopeptides. We speculated that reversing the direction of a 3_{10}-helical peptide bridge could affect (i) the electrochemical behavior of the two electroactive moieties, that is, fullerene and nitroxide, (ii) the interaction between the nitroxide and the fullerene excited state, and (iii) the overall behavior of the couple in terms of nuclear magnetic resonance and electron paramagnetic resonance behaviors.

We synthesized two series of compounds in which the peptide scaffold has a length sufficient to form two intramolecular C═O···H−N hydrogen bonds, based on the 3_{10}-helical structure. The results obtained with the actual fullerene−peptide−radical systems were compared to the behaviors of the corresponding systems lacking either the C_{60} or the free radical moieties but still retaining the same number of intramolecular hydrogen bonds. The numbers **1**, **2**, and **3** are associated with the full fullerene−peptide−radical systems, the corresponding fullerene−peptides, and the radical−peptide systems, respectively (cf., Chart 1). The two series are defined as plus and minus, and the compounds are labeled with "+" or "−" depending on whether the positive or negative side of the peptide dipole moment is directed toward or away from the C_{60} moiety, respectively. The free radical of choice was a nitroxide amino acid derivative (2,2,6,6-tetramethylpiperidine-1-oxyl-4-amino-4-carboxylic acid, TOAC), which also is a C^{α}-tetrasubstituted α-amino acid and thus obeys the same general rules of Aib.[18] This free radical is characterized by a piperidinic ring stabilized by the presence of two contiguous tetrasubstituted carbons.[23] The properties of the two series were studied and compared by IR absorption spectroscopy, electrochemistry, ^{1}H NMR spectroscopy, and EPR spectroscopy.

Electrochemical analysis and chemical reduction experiments (for the nitroxide-bearing molecules) show that the dipole moment of the helix significantly affects the redox behavior of the relevant groups. IR and NMR conformational analysis in solution provides evidence of a folded helical conformation and highlights a specific interaction of one of the helical orientations with the C_{60} moiety. Analysis of the time-resolved EPR (TR-EPR) spectra indicates that quenching of the C_{60} triplet by a

dx.doi.org/10.1021/ja303696s | J. Am. Chem. Soc. 2012, 134, 10628−10637

nitroxide radical occurs efficiently by a radical−triplet pair (RTP) mechanism controlled by the peptide orientation. Therefore, the investigated molecules are better defined as fullerene−peptide−radical systems rather than "simple" fullerene−radical dyads to stress the active role of the bridge not only as a component separating the two moieties and affecting their communication, but also as an important ingredient capable of tuning the system's physicochemical properties significantly.

EXPERIMENTAL SECTION

Chemicals. Unless stated otherwise, all commercially available chemicals were used as received. The syntheses of precursors and peptides **1+**, **2+**, **3+**, **1−**, **2−**, **3−**, and **4** are described in the Supporting Information. The following acronyms will be used: ACN, acetonitrile; Ala, alanine; Boc, *tert*-butyloxycarbonyl; DCE, 1,2-dichloroethane; DEA, diethylamine; DIEA, *N*,*N*-diisopropylethylamine; EDC·HCl, *N*-ethyl-*N*′(3-dimethylaminopropyl)carbodiimide hydrochloride; Fp, 3,4-fulleropyrrolidine; Fmoc, *N*-9-fluorenylmethoxycarbonyloxy; HOAt, 7-aza-1-hydroxybenzotriazole; Piv, pivaloyl (*tert*-butylcarbonyl); TFA, trifluoroacetic acid; Z, benzyloxycarbonyl; trityl, triphenylmethyl.

Infrared Absorption Spectroscopy. Both the solid-state (KBr disk technique) and the solution ($CHCl_3$, cells with 1 mm optical path length, CaF_2 windows) IR absorption spectra were recorded with a Perkin-Elmer model 1720X FT-IR spectrophotometer, nitrogen-flushed, equipped with a sample-shuttle device, at 2 cm^{-1} nominal resolution, and averaging 100 scans.

^{1}H Nuclear Magnetic Resonance Spectroscopy. ^{1}H NMR spectra were obtained with a Bruker model Ascend 500 spectrometer, operating at 500 MHz, or with a Bruker model AC 200 spectrometer, operating at 200 MHz. Deuteriochloroform (99.8%, Aldrich), acetonitrile-d_3 (99.8%, Aldrich), methanol-d_4 (99.8%, Euriso-Top), dimethyl sulfoxide-d_6 (99.8%, Euriso-Top), and water-d_2 (99.8%, Fluka) were used as the solvents. Chemical shifts (δ) are given as parts per million (ppm) downfield from tetramethylsilane, which was added to each solvent as the internal standard. Well-resolved ^{1}H NMR spectra of compounds containing the TOAC moiety were obtained by reduction of the nitroxide with $Na_2S_2O_4$[24] or, for the fullerene derivatives, with diphenylhydrazine.[25] Splitting patterns are abbreviated as follows: (s) singlet, (d) doublet, (t) triplet, (q) quartet, (m) multiplet. The proton assignments were carried out by standard chemical shift correlations as well as by 2D rotating frame nuclear Overhauser effect spectroscopy (ROESY) experiments in deuteriochloroform (for the compounds without TOAC).

Electrochemistry. A CHI 660c electrochemical workstation was used for both differential pulse voltammetry (DPV) and cyclic voltammetry (CV) experiments. The solvent/electrolyte system was DCE containing 0.1 M tetra-*n*-butylammonium hexafluorophosphate (TBAH). All electrochemical experiments were conducted under an argon atmosphere in an all-glass microcell that was thermostatted at 25 °C. The electrochemical experiments were carried out with a homemade glassy carbon (GC) electrode prepared by sharpening a 3 mm diameter Tokai GC-20 rod to obtain a disk with a radius of 0.56 mm. The electrode was prepared as already described.[26] Before experiments, the electrode was polished with 0.015 μm alumina, ultrasonically rinsed with ethanol for 5 min, washed with acetone, and carefully dried with a cold air stream. The electrode was electrochemically activated in the background solution by means of several voltammetric cycles at 0.5 V s^{-1} between the anodic and cathodic potential limits of concern. The electrode area, 9.8×10^{-3} cm^2, was determined by measuring the voltammetric current for the oxidation of ferrocene in *N*,*N*-dimethylformamide/0.1 M tetra-*n*-butylammonium perchlorate, in which ferrocene has a diffusion coefficient of 1.13×10^{-5} cm^2 s^{-1}. A Pt wire was the counter electrode, and an Ag wire was used as a quasi-reference electrode. The Ag wire was kept in a tube filled with the same electrolyte solution but separated from the main working vessel by a Vycor frit. The behavior of the electrode and the quality of the solvent/electrolyte system were first checked in the background solution by using CV. At the end of each experiment, the reference electrode potential was calibrated against the ferricenium/ferrocene (Fc^+/Fc) couple. For DPV, we used a peak amplitude of 50 mV, a pulse width of 0.05 s, 2 mV increment per cycle, and a pulse period of 0.1 s. For the CV experiments, we employed the feedback correction to minimize the ohmic drop between the working and the reference electrodes.

Electron Paramagnetic Resonance. For monitoring the reduction of TOAC in the experiments with diphenylhydrazine in $CHCl_3$, continuous wave electron paramagnetic resonance (CW-EPR) spectra were acquired using a continuous wave Bruker ER 04 XG X-band spectrometer. EPR spectra were recorded with 100 kHz field modulation, 10 dB of 200 mW microwave power, 0.10 mT modulation amplitude, 10.24 ms time constant, and 81.92 ms conversion time. CW-EPR spectra were recorded at different times after addition of diphenylhydrazine. The concentration of the nitroxide was calculated by digital double integration of the CW-EPR spectrum, and the ratio between the integral value before and after addition of diphenylhydrazine was calculated to obtain the % reduced nitroxide value.

For TR-EPR measurements, 0.5 mM **1+** or **1−** in $CHCl_3$ was placed in a 5 mm o.d. quartz tube, carefully degassed by several freeze−pump−thaw cycles, and sealed under vacuum conditions (10^{-3} Torr). A pulsed laser beam from a Nd:YAG laser (Quantel Brilliant, pulse length 5 ns, pulse energy 5 mJ, pulse repetition rate 20 Hz) was used for the optical excitation of the samples at 532 nm, where C_{60} absorption is significantly larger than for nitroxides. Measurements were carried out on a Bruker ER200D (X-band) spectrometer with an extended detection bandwidth (6 MHz), disabling magnetic field modulation and working in direct detection mode. The temperature of the sample inside the EPR cylindrical cavity (8 mm optical access) was controlled by a variable-temperature nitrogen flow system. The time-dependent EPR signals were digitized using a digital oscilloscope (LeCroy model LT344) with a maximum acquisition rate of 500 Megasamples/s synchronized with the laser pulse. The time resolution of the instrument was ca. 150 ns. Data collection was performed with a personal computer and software that allowed controlling the magnetic field and setting the digital oscilloscope. Typically, 300 transient signals were averaged at on-resonance conditions and subtracted from those accumulated off-resonance to eliminate the background signal induced by the laser pulse. A complete two-dimensional (2D) data set that shows the EPR signal as a function of both time and magnetic field consists typically of a set of transient signals, containing 500 points each, recorded at 128 different magnetic field positions. The 400×128 matrix gave a two-dimensional timefield data set from which transient spectra were extracted. CW-EPR spectra have been simulated with the Easyspin package using the "garlic" module for isotropic and fast-motional CW-EPR spectra of radicals in solution.[27] Simulation of transient EPR spectra was carried out using a homemade program compatible with the Easyspin package and based on the RTP mechanism theory.

RESULTS AND DISCUSSION

Synthesis of the Peptides. The fullerene−peptides were synthesized by solution-phase step-by-step procedures, as schematized in Charts 2 and 3. Fp-Ala-(aminoacid)$_3$-NH*t*Bu **1+** and **2+**, and Piv-(Aib)$_2$-(TOAC)-NH*t*Bu **3+** were prepared by coupling the appropriate N^{α}-deprotected peptides H-(aminoacid)$_3$-NH*t*Bu with freshly prepared Fp-Ala-OH and Piv-Cl, respectively. For compounds **1−**, **2−**, and **3−**, the corresponding Piv-peptides with free C-terminal carboxylic group were obtained by removal of OMe protective group by NaOH. Amide coupling between Piv-(aminoacid)$_3$-OH with freshly prepared H-Ala-Fp or *t*BuNH$_2$ yielded Piv-(aminoacid)$_3$-Ala-Fp and Piv-TOAC-(Aib)$_2$-NH*t*Bu, respectively.

The functionalization of C_{60} for obtaining compounds **1+** and **2+**, and **1−** and **2−** was performed as illustrated in Chart 4. Whereas for the minus series we followed a published

dx.doi.org/10.1021/ja303696s | J. Am. Chem. Soc. 2012, 134, 10628−10637

Chart 2. Reaction Scheme for the Synthesis of Fullerene–Peptides 1+ and 2+[a]

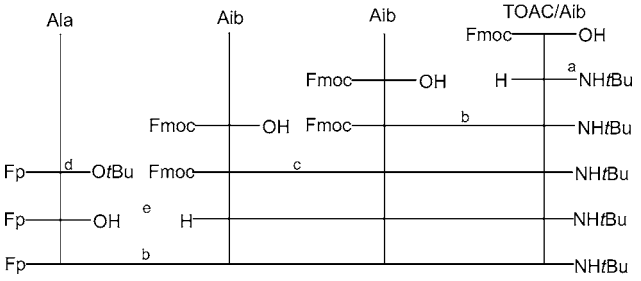

[a](a) Activated ester formation with EDC/HOAt followed by treatment with excess of tBuNH$_2$. (b) Coupling with EDC/HOAt. (c) Removal of Fmoc with DEA/ACN followed by coupling with EDC/HOAt. (d) C_{60}, paraformaldehyde, and HOOC–CH$_2$–NH–CHCH$_3$–COOtBu in refluxing toluene. (e) Removal of tBuO with TFA/CHCl$_3$ and removal of Fmoc with DEA/ACN.

Chart 3. Reaction Scheme for the Synthesis of Fullerene–Peptides 1− and 2−[a]

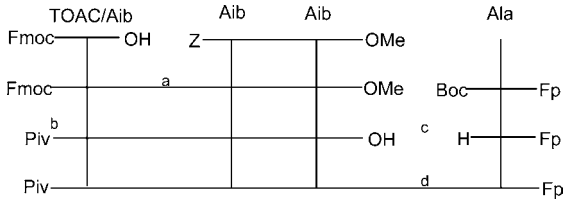

[a](a) Removal of Z with H$_2$/(Pd) in MeOH followed by coupling with EDC/HOAt. (b) Removal of Fmoc with DEA/ACN followed by treatment with Piv-Cl. (c) Removal of OMe with 6 N NaOH/H$_2$O/MeOH and removal of Boc with TFA/CHCl$_3$. (d) Coupling with EDC/HOAt.

procedure,[16] for the plus series we allowed the appropriate *N*-substituted glycine to react with formaldehyde to yield an azomethine ylide that then undergoes a [3 + 2] cycloaddition onto the double bonds of two adjacent C_{60} hexagons.[28] For the synthesis of the TOAC containing peptides, the strategy based on the base-labile Fmoc protecting group was used due to the lability of the nitroxide group under the conditions required for the removal of other protecting groups.[29] On the other hand, only acid-labile protecting groups were used for handling the fullerene derivatives, which are sensitive to basic and reducing conditions.[30]

IR Absorption Spectroscopy. The secondary structure of Aib-containing peptides is conveniently studied by inspection of the IR absorption spectra of the amide A region, pertaining to the stretch of the N–H groups, and the amide 1 region, mostly related to C=O stretching.[18,31] The amide A region of peptides **1+**, **2+**, and **3+** (Figure 1) and peptides **1−**, **2−**, and **3−** (Figure 2) shows a strong absorption band with its maximum in the range 3368 ÷ 3329 cm^{-1} and weaker bands in

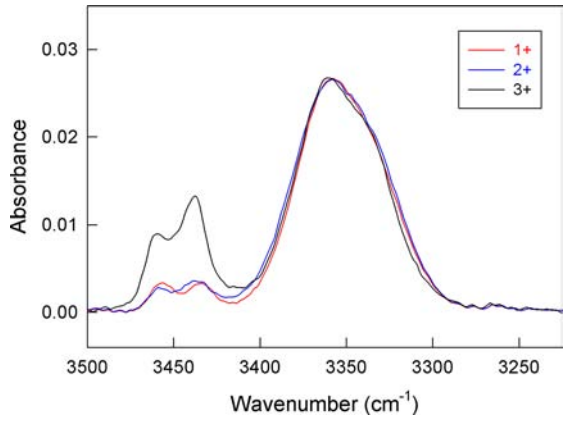

Figure 1. FT-IR absorption spectra for the amide A region of the plus series in CHCl$_3$ at 23 °C: **1+** (red), **2+** (blue), and **3+** (black). The spectra were background subtracted and then normalized with respect to the main N–H band.

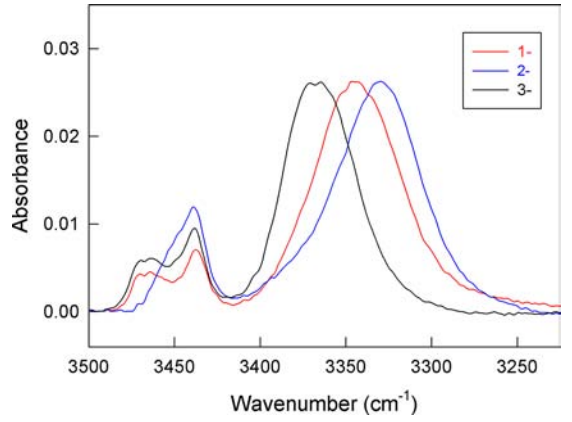

Figure 2. FT-IR absorption spectra for the amide A region of the minus series in CHCl$_3$ at 23 °C: **1−** (red), **2−** (blue), and **3−** (black). The spectra were background subtracted and then normalized with respect to the main N–H band.

Chart 4. Reaction Schemes for the Synthesis of the Precursors for the Plus and Minus Series.

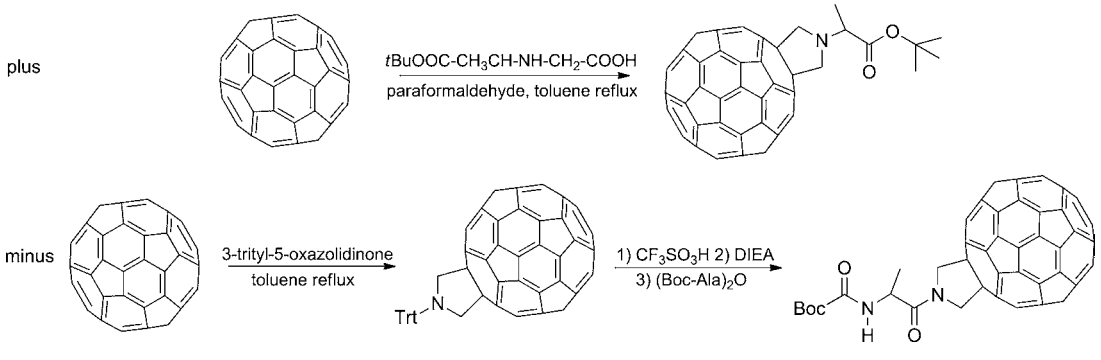

dx.doi.org/10.1021/ja303696s | J. Am. Chem. Soc. 2012, 134, 10628–10637

the range 3470 ÷ 3434 cm^{-1}. These values are typical IR features of folded Aib-peptides: whereas the stronger band is due to intramolecularly H-bonded N−H groups, the weak bands pertain to free N−H groups (in solvents showing no propensity to behave as hydrogen-bond acceptors such as $CHCl_3$, used in our experiments). The spectra of the peptides of the plus series (Figure 1) show a very similar band for the intramolecularly bounded NH groups. On the other hand, a marked difference is evident for the free NH band of peptide−reference **3+**, which is significantly more intense as compared to that of fullerene−peptides **1+** and **2+**. This difference, which is not evident for the peptides of the minus series (cf., Figure 2), points to a different number of free NH groups, and is conceivably related to the presence of the fullerene moiety in **1+** and **2+**. Concerning the minus series, the strong band of **3−** appears at a wavenumber (3367 cm^{-1}) similar to that of the plus series (~3360 cm^{-1}), in line with the wavenumber expected for two intramolecular H-bonds in 3_{10}-helical peptides.[20,31,32] A red shift of such band is observed for **1−** (3344 cm^{-1}) and **2−** (3329 cm^{-1}). The absence of such a shift in the FT-IR spectra of the fullerene peptides of the plus series may indicate a higher sensitivity of the peptide structure of the minus series to the presence of the fullerene moiety.

The amide I region of the two peptide series shows a strong band with its maximum at 1672 ÷ 1662 cm^{-1} (Supporting Information, Figure S2): these wavenumbers are in keeping with carbonyls of a peptide backbone in helical conformation, and a component at higher energy 1681 ÷ 1679 cm^{-1}, particularly evident with **3+** and **3−**, is related to free peptide carbonyls.[18,31] Overall and despite the limited length of the peptide structures investigated, analysis of the amide I region points to relatively stable helical peptides structures with pronounced 3_{10}-helical character.

Electrochemistry. The electrochemical measurements were carried out by cyclic voltammetry (CV) and differential pulse voltammetry (DPV), with a GC electrode and in DCE/0.1 M TBAH. Because the solvent employed has a limited cathodic discharge potential, the analysis focused on the first three reduction peaks of the fullerene moiety of **1+**, **2+**, **1−**, and **2−**. For all peaks, analysis of the CV and DPV peak potentials is in agreement with fully reversible one-electron processes,[33] as expected.[34] The formal potential (E°) values (Table 1) were

Table 1. Formal Potentials of the Investigated Peptides in DCE/0.1 M TBAH at 25 °C[a]

peptide	E°_{1red} (V)	E°_{2red} (V)	E°_{3red} (V)	E°_{ox} (V)
1+	−1.056	−1.458	−1.973	0.202
2+	−1.056	−1.458	−1.972	
3+				0.210
1−	−1.073	−1.460	−1.974	0.283
2−	−1.070	−1.457	−1.972	
3−				0.300
4				0.262

[a]Potentials are against the Fc^+/Fc redox standard.

obtained as the average of the cathodic and anodic CV peak potentials. Figure 3 compares the CV behaviors of **2+** and **2−** (a very similar comparison is valid for **1+** and **1−**), indicating that the E° values of the first peak of the two compounds are different (cf., Table 1). Apart from the different orientation of the peptide bridge, one distinction between the plus and the minus series concerns the chemical bond involving the

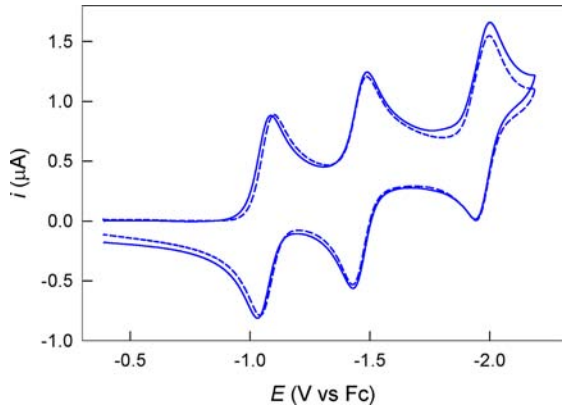

Figure 3. Background-subtracted CV curves of 1 mM **2+** (—) and **2−** (– – –), in DCE/0.1 M TBAH at a scan rate of 0.1 V/s.

fulleropyrrolidine nitrogen: whereas in compounds **1−** and **2−** an amide bond is present, a tertiary amino group characterizes compounds **1+** and **2+** (Chart 1). On the basis of simple substituent-effect considerations, one would thus expect the reduction of C_{60} in **1−** and **2−** to occur at less negative potentials than that of **1+** and **2+**. For example, a positive potential shift of 50 mV was observed on going from *N*-methyl-fulleropyrrolidine to *N*-acyl-fulleropyrrolidine.[35] The outcome of our CV experiments, however, highlights an opposite effect; that is, the first reduction peaks of **1+** and **2+** are less negative by 17 and 14 mV with respect to those of **1−** and **2−**, respectively. The observed potential shift is thus consistent with the effect brought about by the peptide dipole moment.[13] The peak-potential difference fades away for the second and third reduction peaks of fullerene, suggesting that the dipole moment effect is negligible for charged species. Concerning the CVs of both **1+** and **1−** at negative potentials, the only relevant difference with respect to those of **2+** and **2−** is the presence of a shoulder before the third reversible reduction peak of C_{60} (Supporting Information, Figure S3; for the corresponding DPV, see Figures 4 and S4), which is due to the irreversible reduction of the nitroxide radical function, as was also verified in comparison with the CV behavior of **3+** and **3−**, which only carry the nitroxide group.

On the oxidation side, a single reversible oxidation peak is observed. This is due to the oxidation of the TOAC nitroxide radical to the oxoammonium cation.[36] The DPV curves of

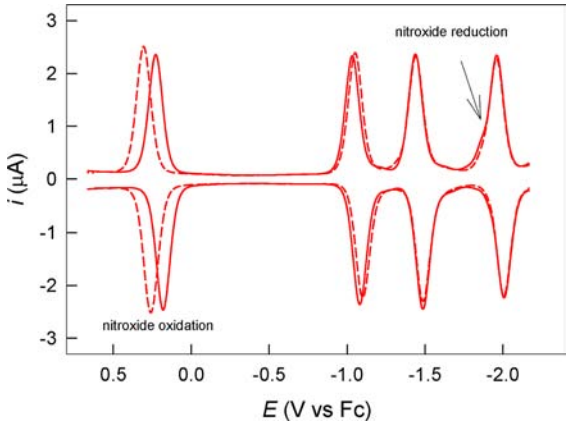

Figure 4. DPV curves of **1+** (—) and **1−** (– – –) in DCE/0.1 M TBAH.

dx.doi.org/10.1021/ja303696s | J. Am. Chem. Soc. 2012, 134, 10628−10637

Figure 4 show that nitroxide oxidation in **1+** is considerably easier than that of **1−** by 80 mV. Therefore, the E° shift is, once again, consistent with the direction expected on the basis of the dipole moment effect: the nitroxide group of **1+** is on the negative side of the peptide dipole, which makes its oxidation easier. To check that the E° shift is indeed independent of the presence of the fullerene moiety and only due to the peptide dipole-moment orientation, we carried out the corresponding CV analysis of peptides **3+** and **3−**. Whereas the oxidation peaks of **3+** and **3−** are slightly more positive than those of **1+** and **1−** (by 8 and 17 mV, respectively), the potential difference is 90 mV and in very good agreement with that between **1+** and **1−**. These results confirm a considerable effect exerted by the helix dipole moment on the energy of the TOAC's molecular orbital hosting the unpaired electron. It is also interesting to compare the oxidation potentials of peptides **3+** and **3−** with that of another TOAC derivative, Boc-TOAC-NH*t*Bu (**4**), which besides lacking the fullerene moiety also does not possess an oriented dipole moment. In keeping with our observations and interpretation, the E° oxidation potential of **4** occurs at 0.262 V, that is, between the values observed for nitroxide oxidation in the plus and minus series (Table 1 and Figure 5). Overall, comparative analysis of the electrochemical

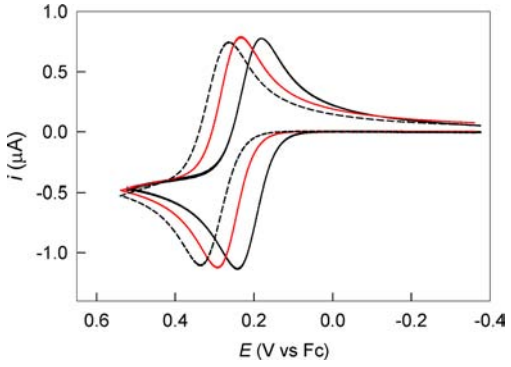

Figure 5. Background-subtracted CV curves of **3+** (—), **3−** (– – –), and **4** (red –), in DCE/0.1 M TBAH and at a scan rate of 0.1 V/s.

behaviors of the investigated peptides points to the important role played by helix dipole on the redox potentials, which reflects a different charge distribution induced by the helix dipole and its effect on the energy of fullerene's lowest unoccupied molecular orbital (LUMO) and TOAC's singly occupied molecular orbital (SOMO).

^{1}H NMR Spectroscopy. The presence of the free radical in compounds **1+** and **1−** makes the analysis of their NMR spectra complicated due to the paramagnetic relaxation enhancement.[37] As a first step in this direction, we used ^{1}H NMR (Figures S5 and S6) and ROESY (Figures S7−S10) to obtain useful insights into the peptide secondary structure of their analogues **2+** and **2−**, where Aib replaces TOAC. ROESY experiments were used to detect through-space connectivities of both the $C^\beta H(i-1)\rightarrow NH(i)$ (between the methyl protons and amide protons of contiguous Aib units) and the $NH(i)\rightarrow NH(i+1)$ types (amide protons of contiguous Aib units). In this way, it was possible to identify the four amide protons of both peptides (cf., Supporting Information). In addition, the $NH(i)\rightarrow NH(i+1)$ cross peak signals indicate that both compounds adopt a prevailing folded structure in keeping with the pattern expected for the 3_{10}-helix. The experiments were carried out in chlorinated solvents ($CDCl_3$ or CD_2Cl_2) incapable of acting as H-bond acceptors: a good test of the participation of peptide amide protons in intramolecular hydrogen bonds is to add a good H-bond acceptor such as Me_2SO-d_6 and to analyze how the ^{1}H NMR spectrum changes.[20] Both N(1)H and N(2)H protons of peptide **2−** were found to be very sensitive to stepwise addition of Me_2SO-d_6, as their resonances underwent significant downfield shifts (Figure 6). On the other hand, the resonances of the two other

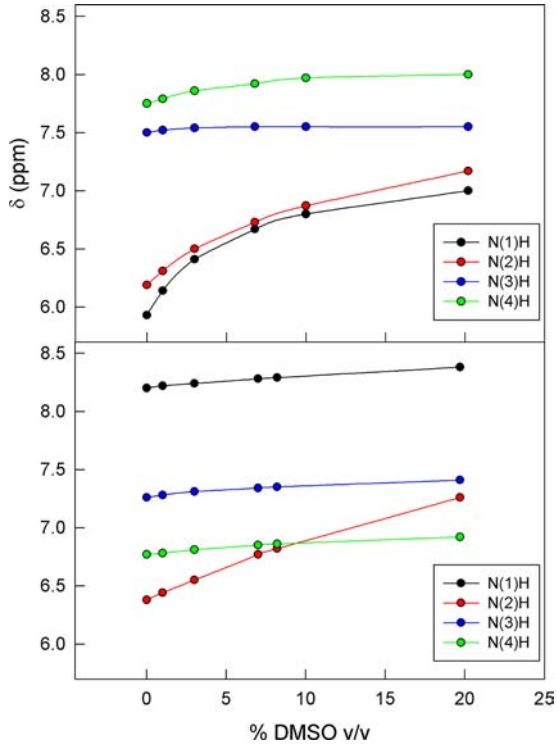

Figure 6. ^{1}H NMR titration in $CDCl_3$. Variation of the chemical shifts of the four amide protons of 1 mM **2−** (upper graph) and **2+** (lower graph) as a function of the addition of Me_2SO-d_6.

amide protons were essentially insensitive, which indicates that Me_2SO-d_6 fails to disrupt the intramolecular H-bonds involving them. Because in the 3_{10}-helix the formation of stable intramolecular H-bonds starts from the N(3)H proton,[18,20] from the sensitivity of the first two NH protons to Me_2SO-d_6 addition, together with the insensitivity of the other NH protons, we infer that peptide **2−** adopts such an ordered secondary structure. The NMR analysis is thus in agreement with the outcome of the IR absorption spectroscopy analysis. As far as peptide **2+** is concerned, the behaviors of the resonances of N(2)H, N(3)H, and N(4)H protons are qualitatively similar to that of **2−**, and thus we can infer a similar ordered structure as supported by the outcome of the IR analysis.

One important difference between the two peptides **2+** and **2−**, however, concerns the very distinct behavior of N(1)H of peptide **2+**. As compared to its usual position in a variety of 3_{10}-helical peptides (around 6 ppm), this resonance was observed at significantly low fields (8.17 ppm). Furthermore, its chemical shift does not depend on Me_2SO-d_6 addition. This indicates that Me_2SO-d_6 does not interact significantly with this otherwise free NH group, as it does with the N(2)H proton. This finding implies that the N(1)H protons are already involved in some sort of rather strong interaction. We observed

dx.doi.org/10.1021/ja303696s | J. Am. Chem. Soc. 2012, 134, 10628−10637

a very similar effect for Aib-peptide monolayer protected gold nanoclusters, in which strong interchain H-bonds between the two otherwise free NH protons of the 3_{10}-helix and C═O groups of neighboring peptide chains form.[32] For peptide **2+**, it is conceivable that the interaction is between N(1)H and the π-system of fullerene,[38] which is possible because of the favorable orientation of the NH groups of **2+**. Consistent with this general conclusion is the outcome of the IR absorption analysis showing that in the amide A region the bands pertaining to free NH groups of both **2+** and **1+** are significantly less intense than those for **3+**, which does not contain the fullerene moiety. The free NH groups of the whole minus series do not present this feature because the free NH groups are on the other side of the fullerene–peptide system and oppositely oriented.

Nitroxide Reduction. The ^{1}H NMR spectra of both **1+** and **1−** reduced forms could be acquired after reduction of the nitroxide moiety with diphenylhydrazine (PH),[39] as we detailed very recently.[25] For both **1+** and **1−**, the presence of the free radical was proved by CW EPR spectra (Figures S16 and S17), which show the typical three lines pattern of the nitroxide due to the ^{14}N (I = 1) nuclei hyperfine coupling.[4,5] The reductive quenching of the radical by PH was monitored by the intensity decrease of the CW EPR signal over time (Figures S16 and S17). We found that under the same redox conditions (23 °C, 10 equiv of PH), peptide **1+** undergoes reduction at a rate 4 times slower than that of **1−** (Figure 7). Once again, this is

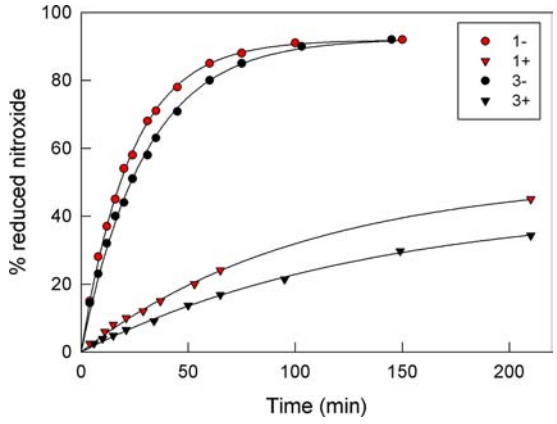

Figure 7. Reduction kinetics for the couples of nitroxide containing compounds **1+** and **3+**, and **1−** and **3−**. The reactions were conducted at 0.05 mM concentration in $CHCl_3$ with 10 equiv of PH, at 23 °C.

nicely in keeping with the effect of the dipole moment: the nitroxides of the minus series (**1−** and **3−**) feel the positive end of the peptide dipole, and this makes their reduction easier.

Figure 8 compares the ^{1}H NMR spectra of compounds **1+** and **2+** and shows the effect brought about by nitroxide reduction on the NMR behavior of **1+**. Before reduction, the ^{1}H NMR spectra of the nitroxide-bearing compounds (see also Figures S13 and S15) only display broad and unresolved peaks in the aliphatic region; no other resonances were observable. After reduction, however, the peaks related to the expected products are resolved and in good agreement with the corresponding behavior of **2+**. A very similar situation holds for the minus series, as illustrated in Figures S11, S12, and S14. Figure 8 shows that, similarly to what was already described for **2+**, also for reduced **1+** the N(1)H proton resonance occurs at very low field (8.18 ppm). On the other hand, this resonance shifts upfield for peptide **3+** (Figure S15), which does not

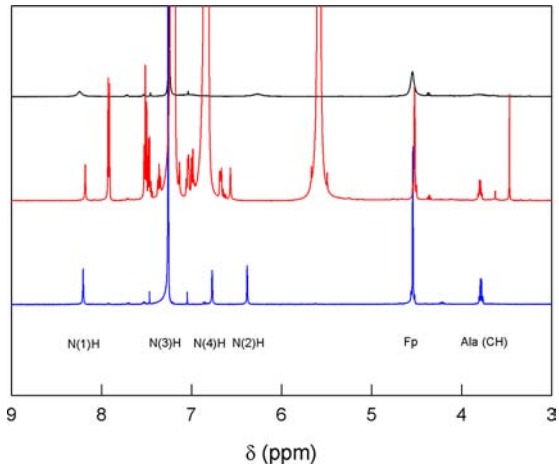

Figure 8. 500 MHz ^{1}H NMR in the NH resonance region of 2 mM **1+** and **2+** in $CDCl_3$ at room temperature. The spectra correspond (from top to bottom) to **1+** before and after reduction of the nitroxide with 50 equiv of PH, and **2+**. N(3)H overlaps the peak of residual chloroform. The peaks at 5.58, 6.85, 7.21, 7.53, and 7.93 ppm belong to PH, which was in excess, and products from its oxidation.[39]

contain the fullerene moiety. The chemical surrounding for the N(1)H proton of **1+** and **2+** is thus the same, in which both protons experience a deshielding effect due to their interaction with C_{60}.[40]

These effects are absent for the minus series, in which the free NH groups are on the other side of the molecule with respect to C_{60} and the orientation of the N–H groups is opposite to that of the plus series. Most of the other features are common to both series: the peaks corresponding to the methylene groups of the TOAC piperidinyl ring appear as two multiplets centered at 2.2 and 2.36 ppm for **1−** (Figures S12 and S14) and at 2.28 and 2.49 ppm for **1+** (Figures S15) in good agreement with the corresponding peaks of **3−** and **3+** (Figures S14 and S15); the resonances of the four TOAC methyl groups are at higher fields, that is, in the range 1.31–1.68 ppm for **1−** and in the range 1.22–1.60 ppm for **1+** (Figures S12, S14, and S15).

TR-EPR. In the primary stages of photochemical reactions, short-lived paramagnetic species are usually generated with polarized spin sublevels, that is, with populations of spin sublevels that differ from those at thermal equilibrium. Chemically induced dynamic electron polarization (CIDEP), used for indicating this phenomenon, provides a powerful tool for investigating elementary steps of photochemical reactions.[41] Triplet quenching by stable free radicals[42] can produce spin polarization in the radical spin sublevels, and a RTP mechanism was proposed to explain the polarization effects observed in transient EPR spectra in solution.[43] Most of the published studies focus on spin polarization of nitroxide radicals interacting in solution with excited state molecules.[44] The RTP mechanism was also extended to molecular systems containing a triplet precursor and a free radical connected by chemical bonds or other interactions.[45]

CW-EPR spectra of peptides **1+** and **1−** in $CHCl_3$ at T = 230 K are shown in Figure S18 together with their simulations. The two spectra are very similar and consist of the typical ^{14}N hyperfine triplet of lines.[4,5] The same g-factor (g_R = 2.0058 ± 0.0005) and hyperfine coupling constant (a_N = 15.32 G) were obtained from simulations (cf., caption to Figure S18). By photoexiciting **1+** and **1−**, we obtained TR-EPR spectra

dx.doi.org/10.1021/ja303696s | J. Am. Chem. Soc. 2012, 134, 10628–10637

showing different features (Figure S19). The TR-EPR spectra show the variation of the EPR signal intensity with respect to magnetic field and time axes. Both transient spectra and time evolution signals can be extracted from TR-EPR data surfaces. Figure 9 shows sections of the TR-EPR data surfaces taken at

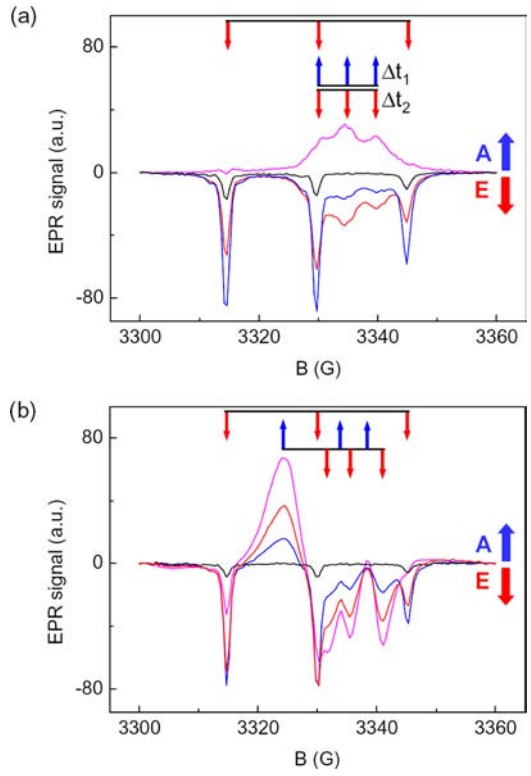

Figure 9. Transient EPR spectra of **1**− (a) and **1**+ (b) in $CHCl_3$ at 280 K, and recorded at increasing time delays after the laser pulse (t = 0.3, 1.4, 2.7, and 10.0 μs for magenta, red, blue, and black spectra, respectively). Both spectra were recorded under the same experimental conditions (microwave power, $P_{\mu w}$ = 10 mW; photoexcitation, λ = 532 nm; E/pulse = 5 mJ). The A and E arrows indicate enhanced absorption and emission polarization, respectively. For both peptides, the polarized signals decay to Boltzmann equilibrium within ca. 28 μs.

increasing time delays after the laser pulse. Immediately after photoexcitation, the transient spectra of **1**− (Figure 9a) consist of the superposition of two triplets of lines with different g factors and hyperfine separations. The first triplet is centered at $g = 2.0064 \pm 0.0005$ (i.e., $g = g_R$ within the experimental error) and is characterized by a line separation of a_N = 15.3 G (nitroxide ^{14}N hyperfine coupling constant). The second triplet at a lower g factor ($g = 2.0033 \pm 0.0005$) consists of three lines with a separation of $a'_N = 4.87\ \text{G} \approx a_N/3$. In the following, the g factor of this second triplet will be indicated as g_Q. Because of the different g factors, the low-field line of the triplet centered at g_Q is superimposed to the central line of the triplet at g_R.[46] The two triplets of lines display different time evolutions. In the early stages after photoexcitation (Figure 9a, magenta spectrum), the three lines of the triplet at g_R are weakly polarized in emission (E),[47] and the emissive character is retained even at longer delays from the laser pulse (Figure 9a, red, blue, and black spectra). On the other hand, the lines assigned to the triplet centered at g_Q show a more complex time evolution: as time increases, the lines reverse their polarization from enhanced absorption (A) to emission. Eventually, while 10 μs after the laser pulse the triplet of lines at g_Q is no more observable, the transient spectrum of **1**− only shows the wider triplet of lines at g_R, with intensities that decrease on going from low to high fields (multiplet effect). A similar TR-EPR spectrum was previously interpreted on the basis of the conventional RTP mechanism.[48]

The TR-EPR spectrum of **1**+ (Figure 9b) shows that after photoexcitation the triplet of lines at g_R has a marked E polarization character. The latter is retained at longer delays, similarly to **1**− (cf., Figure 9a and b, black spectra). Differences between **1**+ and **1**− are evident in the spectra recorded within a few microseconds after photoexcitation and particularly concern several additional reinforced absorptive/emissive polarized components (multiplet with A/E/A/E/A/E polarization pattern) that replace the triplet of lines at g_Q (Figure 9b, magenta, red, and blue spectra). Moreover, no inversion of polarization is observed. This is an unusual TR-EPR behavior previously observed, to the best of our knowledge, only for another nitroxide-C_{60} derivative.[49]

Both of the TR-EPR spectra recorded of **1**− and **1**+ are in keeping with the RTP mechanism theory.[48] According to quantum theory, the coupling of a triplet molecule (S = 1) with a radical (S = 1/2) gives rise to an intermediate RTP that can exist as an excited quartet Q ($Q_{+3/2}$, $Q_{+1/2}$, $Q_{-1/2}$, $Q_{-3/2}$) or doublet D ($D_{+1/2}$, $D_{-1/2}$) spin states, depending on antiparallel or parallel coupling of the two spin systems, respectively. According to the theory, whereas the magnitude of the exchange coupling constant J_0 between the electrons of fullerene and the unpaired electron of nitroxide provides the energy separation between the excited D and Q states of the pair (in particular $E_Q - E_D = 3J_0$), the sign of J_0 determines the ferromagnetic ($J_0 > 0$) or antiferromagnetic ($J_0 < 0$) character of the coupling.[50] Both aspects affect the TR-EPR signal. For both peptides, the triplet of lines at g_R and with separation a_N is assigned to the D ground state transition of the pair separated into three hyperfine components by the nitroxide ^{14}N hyperfine interaction. The emissive polarization character of these three hyperfine lines can be interpreted in terms of quartet-precursor RTP mechanism with $J_0 < 0$.[43] Generally, most RTPs are characterized by a negative J_0, with the positive sign assigned only for particular pairs' geometries[48] or for systems involving some charge transfer contribution to the excited state.[51] The differences of the spectra of **1**− and **1**+ are accounted for by a different intensity of J_0.[52] Two situations, corresponding to weakly and strongly coupled triplet-doublet systems, are possible.[53] The transient spectrum of **1**− (Figure 9a) is interpreted in terms of pure Q and D transitions, that is, by assuming strong coupling ($|J_0| \gg a_N$ = 15 G). On the other hand, the spectra of **1**+ are best interpreted according to a weaker coupling ($|J_0| \leq$ 15 G). Note that transitions between the Q and D states are in principle not allowed, but for **1**+ they are efficient due to the small value of J_0 and thus increased efficient mixing of states. Successful simulation of the transient spectrum of **1**+ (Figure S20)[54] provides full support to the weak-coupling mechanism. A value of J_0 = 7 G was calculated for the exchange coupling constant of this peptide.

These results point to different intensities of the spin exchange coupling between the excited state of fullerene and the radical. The same number of bonds between the fullerene and the radical moieties occurs in both cases, and the interacting spins are at a similar distance (about 10 Å). At such a distance, the exchange interaction is still sensitive to the relative orientation of the fullerene and nitroxide systems. The stronger exchange coupling in **1**− as compared to **1**+, with the

dx.doi.org/10.1021/ja303696s | J. Am. Chem. Soc. 2012, 134, 10628−10637

same (negative) sign, can thus be assigned to different orientations of the pairs in the two cases and thus to the different way by which the helix is oriented. In this context, we note that the line width of the low-field line ($m_i = +1$) hyperfine component in the CW-EPR spectrum of **1+** is slightly larger than that of **1−** (cf., Figure S18). Although small, this difference is in keeping with a less stiff system for **1−**, which provides more opportunities of optimizing the RTP coupling. This result also is in keeping with the IR and NMR results that concur to indicate that **1+** is stiffer because of the NH/fullerene interaction.

CONCLUSIONS

The design, study, and application of new materials with improved physicochemical properties are very important aspects of areas such as molecular electronics, solar cells engineering, and biosensors. In this work, we connected fullerene C_{60} and nitroxide radical moieties with a sufficiently rigid 3_{10}-helical peptide that possesses a strong molecular dipole. The direction of the latter could be reversed by switching the position of fullerene and nitroxide with respect to the peptide's nitrogen and carbon termini. Our main aim was to verify whether this variation would have affected the electrochemical, optical, and magnetic behavior of the fullerene and the nitroxide.

For all of the peptides, FT-IR and NMR analyses provided evidence of highly folded structures, in agreement with the 3_{10}-helix. For the fullerene peptides in which the positive end of the dipole is near C_{60}, the results evidenced a strong interaction between the peptide helix and C_{60}. Analysis of the electrochemical reduction and oxidation of the fullerene and nitroxide groups, respectively, nicely shows that the formal potentials are affected by the peptide dipole in the expected direction. Chemical reduction of the nitroxide radical by diphenylhydrazine was found to proceed with rates that are significantly different for oppositely oriented peptides, once again in keeping with the effect brought about by the peptide dipole. TR-EPR spectra showed that the coupling interaction in triplet quenching by the nitroxide radical can be either weak or strong depending on the orientation of the peptide dipole. Overall, the results point to an important effect of the orientation of the dipole moment and also evidence that the fullerene moiety affects the orientation and, to some extent, rigidity of the peptide chain for one of the two series.

Recently, 3_{10}-helices emerged as particularly convenient rigid spacers or templates to study interactions of molecular moieties possessing tailor-made magnetic, electrochemical, and/or photochemical properties.[55] On the other hand, rigidity also implies the presence of a strong dipole moment.[13,22] In this Article, we show that, although robust peptide helices of this kind (it is worth reminding that peptides based on coded α-amino acids form stable helices only for rather long oligomers) are particularly useful for the design of dyad systems, the orientation of the peptide helix may affect the redox, optical, and magnetic properties of the resulting systems very significantly. Because of these features, the investigated molecules and similar molecular systems should not be described as "simple" fullerene−radical dyads but rather as more complex fullerene−peptide−radical systems, to better stress the active role of the bridge not only as a spacer or a bridge affecting the communication between the two moieties but as an important ingredient for tuning the system's physicochemical properties.

ASSOCIATED CONTENT

Supporting Information

Full details about the syntheses of the peptide and fullerene precursors. Additional electrochemical curves and IR absorption spectroscopy, NMR spectroscopy, and EPR spectra. This material is available free of charge via the Internet at http://pubs.acs.org.

AUTHOR INFORMATION

Corresponding Author

flavio.maran@unipd.it; njt3@columbia.edu

Notes

The authors declare no competing financial interest.

ACKNOWLEDGMENTS

This work was financially supported by the Foundation CARIPARO (progetto di eccellenza), the University of Padova (PRAT grant CPDA103389), and NSF (grant CHE 11-11392). We thank Dr. Steffen Jockusch for his assistance during the nitroxide reduction experiments and Dr. Lorenzo Franco for helpful discussions concerning the TR-EPR experiments and his contribution to simulations.

REFERENCES

(1) Kroto, H. W.; Heath, J. R.; O'Brien, S. C.; Curl, R. F.; Smalley, R. F. *Nature* **1985**, *318*, 162−163.

(2) (a) Karaulova, E. N.; Bagrii, E. I. *Russ. Chem. Rev.* **1999**, *68*, 979−998. (b) Yurovskaya, M. A.; Trushkov, I. V. *Russ. Chem. Bull., Int. Ed.* **2002**, *51*, 367−443. (c) Hirsch, A.; Brettreich, M.; Wudl, F. *Fullerenes: Chemistry and Reactions*; Wiley-VCH: Weinhem, Germany, 2005. (d) Chitta, R.; D'Souza, F. *J. Mater. Chem.* **2008**, *18*, 1440−1471. (e) Kharisov, B. I.; Kharissova, O. V.; Jimenez Gomez, M.; Ortiz Mendez, U. *Ind. Eng. Chem. Res.* **2009**, *48*, 545−571.

(3) (a) Prato, M.; Maggini, M. *Acc. Chem. Res.* **1998**, *31*, 519−526. (b) Maggini, M.; Menna, E. Addition of Azomethyne Ylides: Fulleropyrrolidines. In *Fullerenes: From Synthesis to Optoelectronic Properties*; Guldi, D. M., Martin, N., Eds.; Developments in Fullerene Science, Vol. *4*; Springer: New York, 2003.

(4) (a) Corvaja, C. Electron Paramagnetic Resonance of Modified Fullerenes. In *Fullerenes: From Synthesis to Optoelectronic Properties*; Guldi, D. M., Martin, N., Eds.; Kluwer Academic Publishers: Dordrecht, The Netherlands, 2002; Chapter 7, pp 213−236. (b) Corvaja, C.; Conti, F.; Franco, L.; Maggini, M. *C. R. Chimie* **2006**, *9*, 909−915.

(5) (a) Griffith, O. H.; Cornell, D. W.; Mc Connell, H. M. *J. Phys. Chem.* **1965**, *43*, 2909−2910. (b) Brustolon, M.; Maniero, M.; Corvaja, C. *Mol. Phys.* **1984**, *51*, 1269−1281. (c) *Biological Magnetic Resonance, Spin Labeling - Theory and Applications*; Berliner, L. J., Reuben, J., Eds.; Plenum Press: New York, 1989; Vol. *8*.

(6) Rodriguez-Fortea, A.; Balch, A. L.; Poblet, J. M. *Chem. Soc. Rev.* **2011**, *40*, 3551−3563.

(7) Bakry, R.; Vallant, R. M.; Najam-ul-Haq, M.; Rainer, M.; Szabo, Z.; Huck, C. W.; Bonn, G. K. *Int. J. Nanomed.* **2007**, *2*, 639−649.

(8) Sitharaman, B.; Wilson, L. J. *J. Biomed. Nanotechnol.* **2007**, *3*, 342−352.

(9) Komatsu, K.; Murata, M.; Murata, Y. *Science* **2005**, *307*, 238−240.

(10) Turro, N. J.; Chen, J. Y.-C.; Sartori, E.; Ruzzi, M.; Martí, A.; Lawler, R.; Jockusch, S.; Lopez-Gejo, J.; Komatsu, K.; Murata, Y. *Acc. Chem. Res.* **2010**, *43*, 335−345.

(11) Li, Y.; Lei, X.; Lawler, R. G.; Murata, Y.; Murata, M.; Komatsu, K.; Turro, N. J. *J. Phys. Chem. Lett.* **2010**, *1*, 2135−2138.

(12) (a) Antonello, S.; Formaggio, F.; Moretto, A.; Toniolo, C.; Maran, F. *J. Am. Chem. Soc.* **2003**, *125*, 2874−2875. (b) Polo, F.; Antonello, S.; Formaggio, F.; Toniolo, C.; Maran, F. *J. Am. Chem. Soc.* **2005**, *127*, 492−493.

(13) Holm, A. H.; Ceccato, M.; Donkers, R. L.; Fabris, L.; Pace, G.; Maran, F. *Langmuir* **2006**, *22*, 10584−10589.
(14) (a) Galoppini, E.; Fox, M. A. *J. Am. Chem. Soc.* **1996**, *118*, 2299−2300. (b) Fox, M. A.; Galoppini, E. *J. Am. Chem. Soc.* **1997**, *119*, 5277−5285.
(15) (a) Morita, T.; Kimura, S.; Kobayashi, S.; Imanishi, Y. *J. Am. Chem. Soc.* **2000**, *122*, 2850−2859. (b) Morita, T.; Kimura, S. *J. Am. Chem. Soc.* **2003**, *125*, 8732−8733. (c) Kai, M.; Takeda, K.; Morita, T.; Kimura, S. *J. Pept. Sci.* **2008**, *14*, 192−202. (d) Wain, A. J.; Do, H. N. L.; Mandal, H. S.; Kraatz, H.-B.; Zhou, F. *J. Phys. Chem. C* **2008**, *112*, 14513−14519. (e) Nakayama, H.; Morita, T.; Kimura, S. *Phys. Chem. Chem. Phys.* **2009**, *11*, 3967−3976. (f) Chaudhry, B. R.; Wilton-Ely, J. D. E. T.; Tabor, A. B.; Caruana, D. J. *Phys. Chem. Chem. Phys.* **2010**, *12*, 9996−9998.
(16) Polese, A.; Mondini, S.; Bianco, A.; Toniolo, C.; Scorrano, G.; Guldi, D. M.; Maggini, M. *J. Am. Chem. Soc.* **1999**, *121*, 3446−3452.
(17) de Miguel, G.; Wielopolski, M.; Schuster, D. I.; Fazio, M. A.; Lee, O. P.; Haley, C. K.; Ortiz, A. L.; Echegoyen, L.; Clark, T.; Guldi, D. K. *J. Am. Chem. Soc.* **2011**, *133*, 13036−13054.
(18) Toniolo, C.; Crisma, M.; Formaggio, F.; Peggion, C. *Biopolymers* **2001**, *60*, 396−419.
(19) Crisma, M.; Moretto, A.; Formaggio, F.; Toniolo, C. *Biopolymers* **2006**, *84*, 3−12.
(20) Toniolo, C.; Bonora, G. M.; Barone, V.; Bavoso, A.; Benedetti, E.; Di Blasio, B.; Grimaldi, P.; Lelj, F.; Pavone, V.; Pedone, C. *Macromolecules* **1985**, *18*, 895−902.
(21) Toniolo, C.; Benedetti, E. *Trends Biochem. Sci.* **1991**, *16*, 350−353.
(22) (a) Improta, R.; Barone, V.; Kudin, K. N.; Scuseria, G. E. *J. Am. Chem. Soc.* **2001**, *123*, 3311−3322. (b) Shin, Y.-G.; Newton, M. D.; Isied, S. S. *J. Am. Chem. Soc.* **2003**, *125*, 3722−3732. (c) Wieczorek, R.; Dannenberg, J. J. *J. Am. Chem. Soc.* **2004**, *126*, 14198−14205.
(23) Toniolo, C.; Crisma, M.; Formaggio, F. *Biopolymers* **1998**, *47*, 153−158.
(24) Ozinskas, A. J.; Bobst, A. M. *Helv. Chim. Acta* **1980**, *63*, 1407−1411.
(25) Li, Y.; Lei, X.; Li, X.; Lawler, R. G.; Murata, Y.; Komatsu, K.; Turro, N. J. *Chem. Commun.* **2011**, 12527−12529.
(26) Antonello, S.; Musumeci, M.; Wayner, D. D. M.; Maran, F. *J. Am. Chem. Soc.* **1997**, *119*, 9541−9549.
(27) Stoll, S.; Schweiger, A. *J. Magn. Reson.* **2006**, *178*, 42−55.
(28) Scorrano, G.; Maggini, M.; Prato, M. *J. Am. Chem. Soc.* **1993**, *115*, 9798−9799.
(29) (a) Brook, A. G.; Anderson, D. G.; Duff, J. M.; Jones, P. F.; MacRae, D. M. *J. Am. Chem. Soc.* **1968**, *90*, 1078−1079. (b) Weinkam, R. J.; Jongersen, E. J. *J. Am. Chem. Soc.* **1971**, *93*, 7028−7033.
(30) (a) Wudl, F.; Hirsch, A.; Li, Q. *Ang. Chem., Int. Ed. Engl.* **1991**, 1309−1310. (b) Miller, G. P. *C. R. Chimie* **2006**, *9*, 952−959.
(31) Kennedy, D. F.; Crisma, M.; Toniolo, C.; Chapman, D. *Biochemistry* **1991**, *30*, 6541−6548.
(32) Fabris, L.; Antonello, S.; Armelao, L; Donkers, R. L.; Polo, F.; Toniolo, C.; Maran, F. *J. Am. Chem. Soc.* **2006**, *128*, 326−336.
(33) Bard, A. J.; Faulkner, L. R. *Electrochemical Methods, Fundamentals and Applications*, 2nd ed.; Wiley: New York, 2001.
(34) (a) Wilson, J.; Chibante, F.; Dubois, D.; Kadish, M.; Flanagan, S.; Haufler, R. *J. Am. Chem. Soc.* **1991**, *113*, 4364. (b) Echegoyen, L.; Arias, F.; Xie, Q. *J. Am. Chem. Soc.* **1993**, *115*, 9818−9819.
(35) Prato, M.; Maggini, M.; Giacometti, C.; Scorrano, G.; Sandonà, G.; Farnia, G. *Tetrahedron* **1996**, *52*, 5221−5234.
(36) Eberson, L. *Adv. Phys. Org. Chem.* **1998**, *31*, 91−141.
(37) Rastrelli, F.; Bagno, A. *Chem.-Eur. J.* **2009**, *15*, 7990−8004.
(38) (a) Duan, G.; Smith, V. H.; Weaver, D. F. *J. Phys. Chem. A* **2000**, *104*, 4521−4532. (b) Steiner, T.; Koellner, G. *J. Mol. Biol.* **2001**, *305*, 535−557. (c) Meyer, E. A.; Castellano, R. K.; Diederich, F. *Ang. Chem., Int. Ed.* **2003**, *42*, 1210−1250.
(39) Lee, T. D.; Keana, J. W. *J. Org. Chem.* **1975**, *40*, 3145−3147.
(40) When a proton points directly to the center of an aromatic system, a significant upfield shift is observed in ^{1}H NMR: Cloninger, M. J.; Whitlock, H. W. *J. Org. Chem.* **1998**, *63*, 6153−6159. The opposite is observed for antiaromatic systems. The C_{60} pentagons sustain paratropic currents (deshielding effect) typical of antiaromatic systems: Haddon, R. C. *Science* **1993**, *261*, 1544−1550. Kleinpeter, E.; Klod, S.; Koch, A. *J. Org. Chem.* **2008**, *73*, 1498−1507.
(41) (a) Muus, L. T., Atkins, P. W., McLauchlan, K. A., Pedersen, J. B., Eds. *Chemically Induced Magnetic Polarisation*; Reidel: Dordrecht, The Netherlands, 1977. (b) Salikhov, K. M.; Molin, Y. N.; Sagdeev, R. Z.; Buchachenko, A. L. In *Spin Polarisation and Magnetic Effects in Radical Reactions*; Molin, Y., Ed.; Elsevier: Amsterdam, 1984.
(42) (a) Porter, G.; Wright, M. R. *Discuss. Faraday Soc.* **1959**, *27*, 18−27. (b) Samanta, A.; Kamat, P. V. *Chem. Phys. Lett.* **1992**, *199*, 635−639. (c) Birks, J. B. In *Photophysics of Aromatic Molecules*; Birks, J. B., Ed.; John Wiley: London, 1970; pp 447−449.
(43) Blättler, C.; Jent, F.; Paul, H. *Chem. Phys. Lett.* **1990**, *166*, 375−380.
(44) (a) Kawai, A.; Okutsu, T.; Obi, K. *J. Phys. Chem.* **1991**, *95*, 9130−9134. (b) Kawai, A.; Obi, K. *J. Phys. Chem.* **1992**, *96*, 52−56. (c) Kobori, Y.; Kawai, A.; Obi, K. *J. Phys. Chem.* **1994**, *98*, 6425−6429. (d) Goudsmit, G. H.; Paul, H.; Shushin, A. I. *J. Phys. Chem.* **1993**, *97*, 13243−13249.
(45) (a) Corvaja, C.; Maggini, M.; Prato, M.; Scorrano, G.; Venzin, M. *J. Am. Chem. Soc.* **1995**, *117*, 8857−8858. (b) Corvaja, C.; Maggini, M.; Ruzzi, M.; Scorrano, G.; Toffoletti, A. *Appl. Magn. Reson.* **1997**, *12*, 477−493. (c) Corvaja, C.; Sartori, E.; Toffoletti, A.; Formaggio, F.; Crisma, M.; Toniolo, C.; Mazaleyrat, J. P.; Wakselman, M. *Chem.-Eur. J.* **2000**, *6*, 2775−2782.
(46) Working with the X-band microwave frequency, the g factor difference $g_R - g_Q$ corresponds to ca. 5 G, which is equal to the hyperfine splitting constant a_N'.
(47) Although the spectrum at the magnetic fields corresponding to these lines shows an absorptive character, this absorptive polarization comes from the superimposition of the three emissive lines at g_R with the stronger absorptive polarization of the triplet centered at g_Q.
(48) Mazzoni, M.; Conti, F.; Corvaja, C. *Appl. Magn. Reson.* **2000**, *18*, 351−361.
(49) (a) Franco, L.; Mazzoni, M.; Corvaja, C.; Gubskaya, V. P.; Berezhnaya, L. Sh.; Nuretdinov, I. A. *Mol. Phys.* **2006**, *104*, 1543−1550. (b) Moons, H.; Goovaerts, E.; Gubskaya, V. P.; Nuretdinov, I. A.; Corvaja, C.; Franco, L. *Phys. Chem. Chem. Phys.* **2011**, *13*, 3942−3951.
(50) We assume a spin Hamiltonian of the coupled spin system written as follows: $H_{tot} = \mu_B B_0(g_T S_{T,z} + g_R S_{R,z}) + a_N S_{Rz}\cdot I_z - 2J_0 \boldsymbol{S}_T \boldsymbol{S}_R$, where μ_B is the Bohr magneton, B_0 is the external static magnetic field along the z direction, a_N is the isotropic hyperfine constant of the radical, J_0 is the isotropic exchange coupling constant, and g_R and g_T are the isotropic g-values of the radical and of the triplet species, respectively. Anisotropic interactions are not taken into account because under our experimental conditions (low viscosity liquid solutions at T = 280 K) they are expected to average out.
(51) (a) Kawai, A.; Watanabe, Y.; Shibuya, K. *Mol. Phys.* **2002**, *100*, 1225−1234. (b) Kawai, A. *Appl. Magn. Reson.* **2004**, *26*, 213−221.
(52) van der Est, A.; Asano-Someda, M.; Ragogna, P.; Kaizu, Y. *Phys. Chem. Chem. Phys.* **2011**, *13*, 3942−3951.
(53) This depends on the magnitude of J_0 in comparison with the other magnetic interactions present in the spin system, the hyperfine interaction of the nitroxide (a_N), and the difference in Zeeman interactions between the triplet fullerene and the nitroxide ($\mu_B B_0 g_T - \mu_B B_0 g_R$). If $|J_0| \ll (\mu_B B_0 g_T - \mu_B B_0 g_R)$ and $|J_0| \ll a_N$, the C_{60} triplet and the nitroxide doublet are weakly coupled, and the transient spectrum shows the sum of the two corresponding triplet and radical spectra. On the other hand, for a strong coupling ($|J_0| \gg (\mu_B B_0 g_T - \mu_B B_0 g_R)$ and $|J_0| \gg a_N$), the transient spectrum shows lines involving transitions within the $S = 3/2$ excited states, that is, Q transitions ($Q_{-3/2} \leftrightarrow Q_{-1/2}$, $Q_{-1/2} \leftrightarrow Q_{+1/2}$, $Q_{+1/2} \leftrightarrow Q_{+3/2}$) and D ($D_{-1/2} \leftrightarrow D_{+1/2}$) transitions.
(54) Theoretical details on the simulation program are described in the Supporting Information (caption to Figure S20) and in ref 49a.
(55) Toniolo, C.; Crisma, M.; Formaggio, F.; Peggion, C.; Broxterman, Q. B.; Kaptein, B. *Biopolymers (Pept. Sci.)* **2004**, *76*, 162−176.